SCIENTIFIC REP⬤RTS

The polarization and the fundamental sensitivity of ^{39}K (^{133}Cs)-^{85}Rb-^{4}He hybrid optical pumping spin exchange relaxation free atomic magnetometers

Jian-Hua Liu[1,3], Dong-Yang Jing[1,2], Liang-Liang Wang[1,2], Yang Li[4], Wei Quan[4], Jian-Cheng Fang[4] & Wu-Ming Liu[1,2]

The hybrid optical pumping spin exchange relaxation free (SERF) atomic magnetometers can realize ultrahigh sensitivity measurement of magnetic field and inertia. We have studied the ^{85}Rb polarization of two types of hybrid optical pumping SERF magnetometers based on ^{39}K-^{85}Rb-^{4}He and ^{133}Cs-^{85}Rb-^{4}He respectively. Then we found that ^{85}Rb polarization varies with the number density of buffer gas ^{4}He and quench gas N$_2$, pumping rate of pump beam and cell temperature respectively, which will provide an experimental guide for the design of the magnetometer. We obtain a general formula on the fundamental sensitivity of the hybrid optical pumping SERF magnetometer due to shot-noise. The formula describes that the fundamental sensitivity of the magnetometer varies with the number density of buffer gas and quench gas, the pumping rate of pump beam, external magnetic field, cell effective radius, measurement volume, cell temperature and measurement time. We obtain a highest fundamental sensitivity of $1.5073\ aT/Hz^{1/2}$ ($1\ aT = 10^{-18}\ T$) with ^{39}K-^{85}Rb-^{4}He magnetometer between above two types of magnetometers when ^{85}Rb polarization is 0.1116. We estimate the fundamental sensitivity limit of the hybrid optical pumping SERF magnetometer to be superior to 1.8359×10^{-2} $aT/Hz^{1/2}$, which is higher than the shot-noise-limited sensitivity of $1\ aT/Hz^{1/2}$ of K SERF atomic magnetometer.

In recent years, ultrahigh sensitive magnetic field measurement technology has become a hotspot in research of weak magnetic field. In the field of biomedicine, it is used in magnetoencephalography (MEG) and magneto-cardiography (MCG)[1–3]. In physics, it is used to analyze the magnetism of material and measure the symmetry broken of charge conjugation, parity transformation and time reversal (CPT)[4–6]. At present, the sensitivity of the spin exchange relaxation free (SERF) atomic magnetometer is the highest in the ultrahigh sensitive magneto-meters[3, 7–10]. The shot-noise limit of the K SERF magnetometer[11] is estimated to be $2\ aT/Hz^{1/2}$ and with more optimization, it should be possible to approach the shot-noise-limited sensitivity in the range $10 - 1\ aT/Hz^{1/2}$ for K SERF magnetometer[10]. The effects of the spin-exchange relaxation can be suppressed in the SERF regime, when the spin-exchange rate is much larger than the Larmor precession frequency[12, 13]. The SERF regime can be reached by operating with sufficiently high alkali metal number density (at higher temperature) and in sufficiently low magnetic field[13, 14].

It was found that hybrid optical pumping can make the SERF magnetometer realize higher experimental detecting sensitivity and more homogeneous atomic spin polarization[15] and it is suitable for quantum nondestructive measurement[16]. Ito *et al.*[17, 18] realized a sensitivity of $3 \times 10^4\ aT/Hz^{1/2}$ in magnetic field measurement by

[1]Beijing National Laboratory for Condensed Matter Physics, Institute of Physics, Chinese Academy of Sciences, Beijing, 100190, China. [2]School of Physical Sciences, University of Chinese Academy of Sciences, Beijing, 100190, China. [3]School of Science, Beijing Technology and Business University, Beijing, 100048, China. [4]School of Instrument Science and Opto-Electronics Engineering, and Science and Technology on Inertial Laboratory, Beihang University, Beijing, 100191, China. Correspondence and requests for materials should be addressed to W.-M.L. (email: wliu@iphy.ac.cn)

SERF atomic magnetometers by hybrid optical pumping of K-Rb. Fang *et al.*[19] obtained a sensitivity of approximately 5×10^3 $aT/Hz^{1/2}$ by optimizing the parameters of SERF magnetometer based on K-Rb hybrid optical pumping. Li *et al.*[20] measured the magnetic field sensitivity better than 700 $aT/Hz^{1/2}$ by a subfemtotesla atomic magnetometer based on hybrid optical pumping of K-Rb. However, there is almost no work about the systematic analysis of the influence factors on the polarization and the fundamental sensitivity of K (Cs)-Rb-He hybrid optical pumping SERF atomic magnetometers. We need more practical methods to obtain higher fundamental sensitivity of the hybrid optical pumping SERF atomic magnetometer.

In this report, we obtain a general formula on the fundamental sensitivity of the hybrid optical pumping SERF magnetometer, which describes the fundamental sensitivity of the magnetometer varying with the number density of buffer gas and quench gas, pumping rate of pump beam, external magnetic field, cell effective radius (the shape of the cell is roughly spherical), measurement volume, cell temperature and measurement time. We have investigated two types of hybrid optical pumping SERF atomic magnetometers based on ^{39}K (^{133}Cs)-^{85}Rb-^{4}He (^{39}K (^{133}Cs)-^{85}Rb-^{4}He magnetometers), then found the fundamental sensitivity of ^{133}Cs-^{85}Rb-^{4}He magnetometer is lower than the one of ^{39}K-^{85}Rb-^{4}He magnetometer at the same cell temperature and in the SERF regime when the pumping rate of pump beam is bigger than about 1916 s^{-1} and N$_2$ number density is bigger than about 1.974×10^{16} cm^{-3} at our chosen conditions. Optimizing the magnetometer parameters is advantageous to improve the sensitivity of the magnetometer in measuring weak magnetic field. Furthermore, we obtained a higher fundamental sensitivity of 1.8359×10^{-2} $aT/Hz^{1/2}$ with ^{39}K-^{85}Rb-^{4}He magnetometer when the polarization of ^{85}Rb atom is 1.3174×10^{-4} and the fundamental sensitivity is higher than the shot-noise-limited sensitivity of K SERF atomic magnetometer[10] in the range $10 - 1$ $aT/Hz^{1/2}$. Among ^{39}K, ^{85}Rb and ^{133}Cs SERF magnetometers, there is a maximum temperature range for ^{39}K to make the magnetometer in the SERF regime with the number density of ^{39}K satisfies the condition of the SERF regime, so the SERF magnetometer based on ^{39}K is suitable for an environment with the temperature varying drastically. These findings not only optimize the parameters for the SERF regime, but also provide an experimental guide for the design of the hybrid optical pumping SERF magnetometer.

Results

The number density of alkali-metal atoms.
The alkali metal vapor cell (the shape of the cell is roughly spherical) of the SERF atomic magnetometer based on hybrid optical pumping contains two types of alkali metal atoms, they are ^{39}K-^{85}Rb or ^{133}Cs-^{85}Rb. ^{133}Cs can reach large saturation vapor pressure at lower temperature[21] and realize SERF regime at lower temperature, which has more advantages for low temperature conditions. ^{39}K has the highest theoretical sensitivity, so we study the hybrid optical pumping SERF atomic magnetometers based on ^{39}K-^{85}Rb and ^{133}Cs-^{85}Rb respectively. We select ^{4}He as the buffer gas and take N$_2$ as quench gas (that is ^{39}K (^{133}Cs)-^{85}Rb-^{4}He magnetometers). ^{4}He gas suppresses the spin relaxation caused by wall collisions, colliding with excited alkali metal atoms and absorbing the energy, N$_2$ gas restrains radiative deexcitation of the excited alkali metal atoms[22]. One type of alkali-metal atom which is directly pumped and polarized by a circularly polarized pump beam is called A and the other type of alkali-metal atom which is polarized by the spin-exchange collisions with A is called B in the hybrid optical pumping SERF magnetometer[16, 23], we take ^{39}K or ^{133}Cs as A respectively, select ^{85}Rb as B in the SERF regime. The number density of alkali-metal vapor and the polarization of alkali-metal vapor are two most important parameters of the cell[24].

The saturated density of the alkali-metal atoms vapor in units of cm^{-3} at cell temperature T in Kelvin is given by ref. 5

$$n_{sat} = \frac{1}{T} 10^{21.866 + A_1 - B_1/T},$$

(1)

where n_{sat} is the saturated density of alkali-metal (^{39}K, ^{85}Rb and ^{133}Cs) atom vapor. When the alkali-metal vapor cell only contains one type of alkali-metal atom (single alkali-metal vapor cell), the number density of the alkali-metal atom equals to the saturated density of the alkali-metal atom, the parameters A_1 and B_1 are phase parameters[21], where $A_1^{K} = 4.402$, $A_1^{Rb} = 4.312$, $A_1^{Cs} = 4.165$, $B_1^{K} = 4453$, $B_1^{Rb} = 4040$ and $B_1^{Cs} = 3830$ for the temperature is higher than $400 K$.

We can obtain the number density of ^{39}K, ^{133}Cs and ^{85}Rb varying with the cell temperature for the single alkali-metal vapor cell from equation (1) as shown in Fig. 1. When the number density of ^{39}K, ^{85}Rb and ^{133}Cs atom are the same, ^{39}K need the highest temperature. In general, the number density of the alkali metal atoms is 10^{13} cm^{-3} to 10^{14} cm^{-3} in the SERF regime, we can find that there is a maximum temperature range for ^{39}K to make the magnetometer in the SERF regime with the number density of ^{39}K satisfies the condition of the SERF regime, therefore, the SERF magnetometer based on ^{39}K is suitable for an environment with the temperature varying drastically. If we increase the cell temperature, we can obtain higher number density of alkali-metal atoms, however, the cell glass will be corroded, the laser power and heating equipment will be unable to bear and there will be other problems experimentally when the number density of alkali-metal atoms is greater than or equal to 10^{15} cm^{-3}. What's more, the optical depth will be too big so that the laser will be largely absorbed by the atoms. If the vapor cell is made of special glass, the laser power is very big and the volume of the vapor cell is very small, we can appropriately increase the temperature of the vapor cell. Depending on equation (1), when cell temperature $T = 457.5 K$, for single alkali-metal vapor cell, we obtain the number density of ^{39}K is $n_K = 7.4864 \times 10^{13}$ cm^{-3}, the number density of ^{85}Rb is $n_{Rb} = 9.9776 \times 10^{14}$ cm^{-3}, the number density of ^{133}Cs is $n_{Cs} = 4.8642 \times 10^{14}$ cm^{-3}. When $T = 457.6 K$, we obtain $n_K = 7.5216 \times 10^{13}$ cm^{-3}, $n_{Rb} = 1.0017 \times 10^{15}$ cm^{-3}, $n_{Cs} = 4.8848 \times 10^{14}$ cm^{-3}. Because SERF regime can be reached by operating with sufficiently high alkali metal number density (at higher temperature) and in sufficiently low magnetic field[13, 14], we choose $T = 457.5 K$ as the highest temperature to reduce the corrosion of alkali metal atoms to the vapor cell and make the magnetometer in the SERF regime.
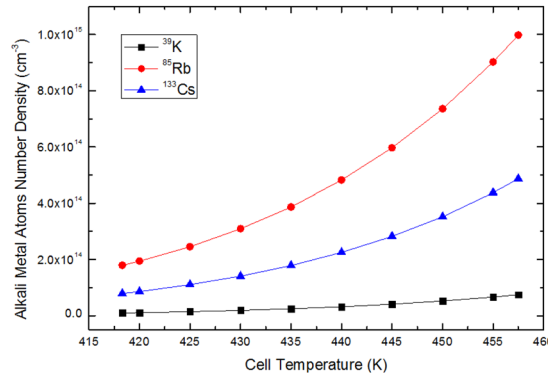
Figure 1. The number density of ^{39}K, ^{133}Cs and ^{85}Rb vary with temperature. Among ^{39}K, ^{85}Rb and ^{133}Cs SERF magnetometers, there is a maximum temperature range for ^{39}K to make the magnetometer in the SERF regime with the number density of ^{39}K (black line in squares) satisfies the condition of the SERF regime, so the SERF magnetometer based on ^{39}K is applicable to the working environment with the temperature varies drastically.

The polarization of alkali-metal atom. Considering the spin-exchange between two types of alkali-metal atoms A and B in the hybrid vapor cell, here, we assume that the vapor densities obey the Raoult's law[25], $n_B \approx f_B n_{sat}{}^B$, where f_B is the mole fraction of atom B in the metal and $n_{sat}{}^B$ is the saturated vapor density for pure atom B metal. When the mole fraction of atom B is 0.97, we can obtain the number density of atom A and B, $n_A \approx 0.03 n_{sat}{}^A$, $n_B \approx 0.97 n_{sat}{}^B$, the spin polarization P of each type of atoms in zero magnetic field can be described as[19],

$$P_A = \frac{R_{SE}^B P_B + R_p}{R_p + R_{SD}^A + R_{SE}^B}, \tag{2}$$

$$P_B = \frac{R_{SE}^A P_A}{R_{SD}^B + R_{SE}^A}, \tag{3}$$

$$R_{SD}^A = n_A \sigma_{SD}^{A-A} \bar{v}_{A-A} + n_{He} \sigma_{SD}^{A-He} \bar{v}_{A-He} + n_{N_2} \sigma_{SD}^{A-N_2} \bar{v}_{A-N_2} + n_A \sigma_{SD}^{A-B} \bar{v}_{A-B}, \tag{4}$$

$$R_{SD}^B = n_B \sigma_{SD}^{B-B} \bar{v}_{B-B} + n_{He} \sigma_{SD}^{B-He} \bar{v}_{B-He} + n_{N_2} \sigma_{SD}^{B-N_2} \bar{v}_{B-N_2} + n_B \sigma_{SD}^{B-A} \bar{v}_{B-A}, \tag{5}$$

where A represents alkali-metal atom ^{39}K or ^{133}Cs, B represents alkali-metal atom ^{85}Rb. R_{SE}^A is the spin-exchange rate of atom B with atom A, $R_{SE}^A = k_{SE} n_A = n_A \sigma_{SE}^{B-A} \bar{v}_{B-A}$, R_{SE}^B is the spin-exchange rate of atom A with atom B, $R_{SE}^B = k_{SE} n_B = n_B \sigma_{SE}^{A-B} \bar{v}_{A-B}$, R_p is the pumping rate of pump beam, which is mainly determined by pumping laser parameters[6], $R_B = k_{SE} n_A P_A$ is the pumping rate of atom B[17], R_{SD} is the spin destruction relaxation rate, k_{SE} is the spin-exchange rate constant, n is the number density of atoms, $\bar{v}_{alkali-alkali}$ is the relative velocity between the alkali atoms, $\bar{v}_{alkali-alkali} = \sqrt{\frac{8\kappa_B T}{\pi m_{alkali-alkali}}}$, κ_B is Boltzmann's constant, T is cell temperature, $\bar{v}_{alkali-N_2} = \sqrt{\frac{8\kappa_B T}{\pi m_{alkali-N_2}}}$ is the relative velocity between the alkali atoms and quench gas N_2 respectively, the reduced mass of alkali atoms and quench gas N_2 is $m_{alkali-N_2} = \frac{m_{alkali} m_{N_2}}{m_{alkali} + m_{N_2}}$, the relative velocity between the alkali atoms and buffer gas ^{4}He is $\bar{v}_{alkali-He} = \sqrt{\frac{8\kappa_B T}{\pi m_{alkali-He}}}$, the reduced mass of alkali atoms and buffer gas ^{4}He is $m_{alkali-He} = \frac{m_{alkali} m_{He}}{m_{alkali} + m_{He}}$, k_{SE} for different alkali metal atoms are nearly the same[26–30], $k_{SE} = \langle \sigma_{SE} v \rangle$, $k_{SE}^{Rb-Cs} = k_{SE}^{Cs-Rb}$, $k_{SE}^{Rb-K} = k_{SE}^{K-Rb}$, the spin-exchange cross section of ^{39}K, ^{85}Rb and ^{133}Cs is $\sigma_{SE}^K = 1.8 \times 10^{-14} cm^2$, $\sigma_{SE}^{Rb} = 1.9 \times 10^{-14} cm^2$ and $\sigma_{SE}^{Cs} = 2.1 \times 10^{-14} cm^2$ respectively[27, 31], $k_{SE}^{Cs-Rb} = \sigma_{SE}^{Cs-Rb} \sqrt{\frac{m_{Rb} + m_{Cs}}{m_{Rb} m_{Cs}}} \sqrt{\frac{8\kappa_B T}{\pi}}$ and $k_{SE}^{K-Rb} = \sigma_{SE}^{K-Rb} \sqrt{\frac{m_{Rb} + m_K}{m_{Rb} m_K}} \sqrt{\frac{8\kappa_B T}{\pi}}$, where σ_{SE}^{K-Rb} is the spin-exchange cross section of ^{39}K and ^{85}Rb by spin-exchange collisions with each other, σ_{SE}^{Cs-Rb} is the spin-exchange cross section of ^{133}Cs and ^{85}Rb by spin-exchange collisions with each other, for $\sigma_{SE}^{87Rb-87Rb} = (1.9 \pm 0.2) \times 10^{-14} cm^2$, $\sigma_{SE}^{87Rb-133Cs} = (2.3 \pm 0.2) \times 10^{-14} cm^2$, however, we don't find the values of $\sigma_{SE}^{39K-85Rb}$ and $\sigma_{SE}^{133Cs-85Rb}$, we take $\sigma_{SE}^{39K-85Rb} = \sigma_{SE}^{85Rb-39K} \approx \sigma_{SE}^K \frac{n_K}{n_K + n_{Rb}} + \sigma_{SE}^{Rb} \frac{n_{Rb}}{n_K + n_{Rb}}$, $\sigma_{SE}^{133Cs-85Rb} = \sigma_{SE}^{85Rb-133Cs} \approx \sigma_{SE}^{Cs} \frac{n_{Cs}}{n_{Cs} + n_{Rb}} + \sigma_{SE}^{Rb} \frac{n_{Rb}}{n_{Cs} + n_{Rb}}$ by considering the weight of ^{39}K, ^{85}Rb and ^{133}Cs.

The spin-destruction cross section of ^{39}K-^{39}K, ^{85}Rb-^{85}Rb and ^{133}Cs-^{133}Cs are $\sigma_{SD}^K = 1 \times 10^{-18} cm^2$, $\sigma_{SD}^{Rb} = 1.6 \times 10^{-17} cm^2$ and $\sigma_{SD}^{Cs} = 2 \times 10^{-16} cm^2$ respectively[32–34], σ_{SD}^{K-Rb}, σ_{SD}^{Rb-K}, σ_{SD}^{Cs-Rb} and σ_{SD}^{Rb-Cs} are the spin-destruction cross section of ^{39}K and ^{85}Rb, ^{85}Rb and ^{39}K, ^{133}Cs and ^{85}Rb, ^{85}Rb and ^{133}Cs by collisions with each other respectively. However, we do not find the values of σ_{SD}^{K-Rb}, σ_{SD}^{Rb-K}, σ_{SD}^{Cs-Rb} and σ_{SD}^{Rb-Cs} in any
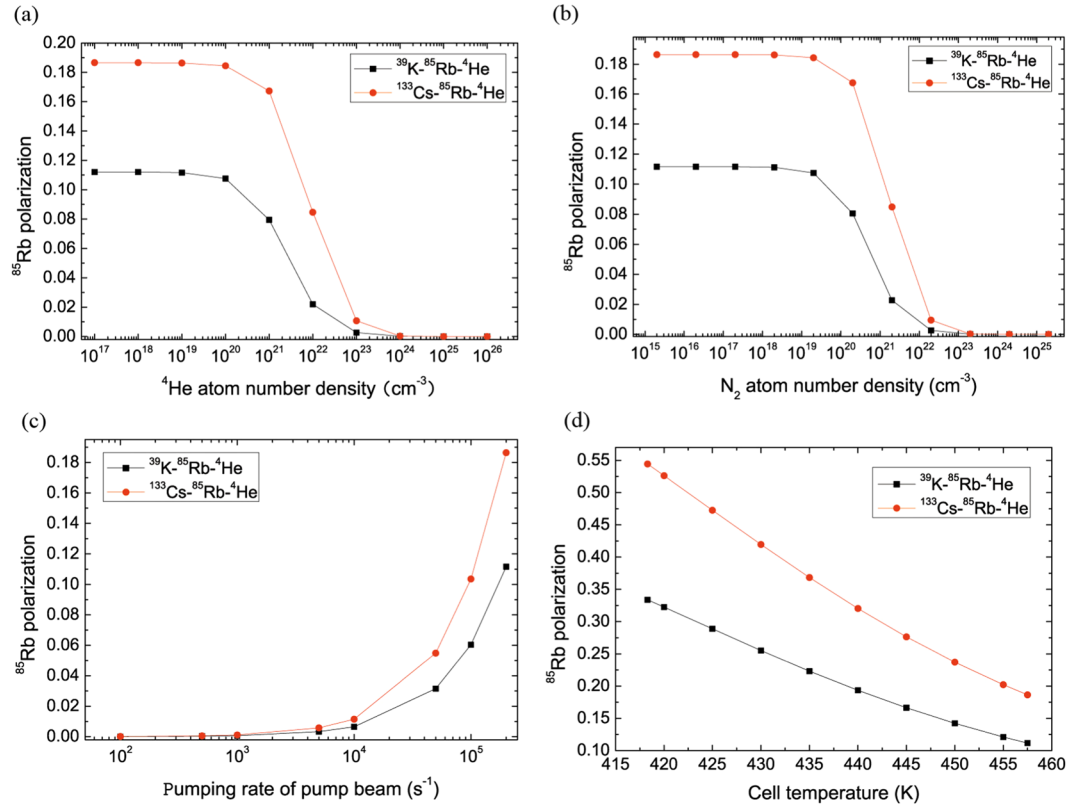
Figure 2. The ^{85}Rb polarization of ^{39}K (^{133}Cs)-^{85}Rb-^{4}He magnetometers varies with the number density of the buffer gas (^{4}He), the pumping rate of pump beam, number density of the quench gas N_2 and the cell temperature respectively. (**a**) ^{85}Rb polarization almost does not vary with the increasing ^{4}He number density when ^{4}He number density is smaller than a critical value about 10^{20} cm^{-3} in ^{39}K -^{85}Rb-^{4}He (black line in squares) and ^{133}Cs-^{85}Rb-^{4}He (red line in dots) magnetometers, otherwise, ^{85}Rb polarization decreases rapidly. (**b**) ^{85}Rb polarization almost does not vary with increasing N_2 number density when N_2 number density is smaller than about 2×10^{19} cm^{-3} in ^{39}K-^{85}Rb-^{4}He and ^{133}Cs-^{85}Rb-^{4}He magnetometers, otherwise, the ^{85}Rb polarization decreases rapidly. (**c**) ^{85}Rb polarization increases with increasing R_p^K and R_p^{Cs} respectively. (**d**) ^{85}Rb polarization decreases with the increasing cell temperature. The ^{85}Rb polarization of ^{133}Cs-^{85}Rb-^{4}He magnetometer is bigger than the one of ^{39}K-^{85}Rb-^{4}He magnetometer in (**a**)–(**d**).

references, depending on the spin-destruction cross section of ^{39}K-^{39}K, ^{85}Rb-^{85}Rb and ^{133}Cs-^{133}Cs, we take $\sigma_{SD}^{K-Rb} = \sigma_{SD}^{Rb-K} \approx \sigma_{SD}^{K} \frac{n_K}{n_K + n_{Rb}} + \sigma_{SD}^{Rb} \frac{n_{Rb}}{n_K + n_{Rb}}$, $\sigma_{SD}^{Cs-Rb} = \sigma_{SD}^{Rb-Cs} \approx \sigma_{SD}^{Cs} \frac{n_{Cs}}{n_{Cs} + n_{Rb}} + \sigma_{SD}^{Rb} \frac{n_{Rb}}{n_{Cs} + n_{Rb}}$ by considering the weight of ^{39}K, ^{85}Rb and ^{133}Cs. The spin-destruction cross section of ^{4}He and ^{39}K, ^{4}He and ^{85}Rb, ^{4}He and ^{133}Cs are $\sigma_{SD}^{K-He} = 8 \times 10^{-25}$ cm^2, $\sigma_{SD}^{Rb-He} = 9 \times 10^{-24}$ cm^2 and $\sigma_{SD}^{Cs-He} = 2.8 \times 10^{-23}$ cm^2 respectively[11]. The spin-destruction cross section of N_2 and ^{39}K, N_2 and ^{85}Rb, N_2 and ^{133}Cs is $\sigma_{SD}^{K-N_2} = 7.9 \times 10^{-23}$ cm^2, $\sigma_{SD}^{Rb-N_2} = 1 \times 10^{-22}$ cm^2 and $\sigma_{SD}^{Cs-N_2} = 5.5 \times 10^{-22}$ cm^2 respectively[11, 35].

Substitute equation (2) into equation (3), we obtain

$$P_B = \frac{R_p R_{SE}^A}{(R_{SD}^B + R_{SE}^A)(R_p + R_{SD}^A + R_{SE}^B) - R_{SE}^A R_{SE}^B},$$

(6)

We take one of ^{4}He number density n_{He}, N_2 number density n_{N2}, cell temperature T and pumping rate of pump beam R_p by equation (6) as a variable (other parameters are invariable) to obtain the results that the polarization of the hybrid optical pumping SERF magnetometer based on ^{39}K (^{133}Cs)-^{85}Rb-^{4}He respectively vary with the variable. Depending on suggestions and the typical conditions of the experiment group[19, 30, 36], in order to facilitate the theoretical analysis, we take the mole fraction of ^{85}Rb $f_{Rb} = 0.97$, $n_{He} = 10^{19}$ cm^{-3}, $n_{N2} = 2 \times 10^{17}$ cm^{-3}, $R_p = R_p^K = R_p^{Cs} = 200000$ s^{-1} and $T = 457.5$ K, at the moment, ^{39}K, ^{85}Rb and ^{133}Cs are in the SERF regime.

The number density of ^{39}K, ^{85}Rb and ^{133}Cs vary with cell temperature and the mole fraction for the hybrid alkali-metal vapor cell, so the relation among the polarization of ^{85}Rb, the number density of alkali metal atom (^{39}K, ^{85}Rb or ^{133}Cs) and cell temperature is nonlinear in groups ^{39}K-^{85}Rb and ^{133}Cs-^{85}Rb when the mole fraction of the alkali-metal atoms are fixed. At the same cell temperature, the number density of ^{39}K, ^{85}Rb and ^{133}Cs are different. When the number density of ^{39}K, ^{85}Rb and ^{133}Cs are equivalent, the cell temperature of ^{39}K-^{85}Rb and

^{133}Cs-^{85}Rb magnetometers are different, and the ^{85}Rb polarization of ^{39}K-^{85}Rb and ^{133}Cs-^{85}Rb magnetometers are also different.

Figure 2 demonstrates the ^{85}Rb polarization of ^{39}K (^{133}Cs)-^{85}Rb-^{4}He magnetometers as a function of ^{39}K, ^{133}Cs, ^{85}Rb, ^{4}He, and N$_2$ number density, the pumping rate of pump beam and cell temperature, including the effects of spin exchange due to ^{39}K-^{85}Rb, ^{85}Rb-^{39}K, ^{133}Cs-^{85}Rb, ^{85}Rb-^{133}Cs and spin relaxation due to ^{39}K-^{39}K, ^{39}K-^{85}Rb, ^{85}Rb-^{85}Rb, ^{133}Cs-^{85}Rb, ^{133}Cs-^{133}Cs, ^{39}K-^{4}He, ^{85}Rb-^{4}He, ^{133}Cs-^{4}He collisons, ^{39}K-N$_2$, ^{85}Rb-N$_2$, ^{133}Cs-N$_2$ destructions. The ^{85}Rb polarization almost does not vary with ^{4}He number density when ^{4}He number density is smaller than a critical value about 10^{20} cm^{-3} in ^{39}K-^{85}Rb-^{4}He (black line in squares) and ^{133}Cs-^{85}Rb-^{4}He (red line in dots) magnetometers, otherwise, the ^{85}Rb polarization decreases rapidly in Fig. 2(a). The ^{85}Rb polarization almost does not vary with N$_2$ number density when N$_2$ number density is smaller than about 2×10^{19} cm^{-3} for ^{39}K-^{85}Rb-^{4}He magnetometer and ^{133}Cs-^{85}Rb-^{4}He magnetometer. Otherwise, the ^{85}Rb polarization decreases rapidly in Fig. 2(b). The ^{85}Rb polarization increases with the increasing pumping rate of pump beam R_p^K and R_p^{Cs} respectively in Fig. 2(c). The polarization of ^{85}Rb decreases with the cell temperature increasing in Fig. 2(d). The ^{85}Rb polarization of ^{133}Cs-^{85}Rb-^{4}He magnetometer is bigger than the one of ^{39}K-^{85}Rb-^{4}He magnetometer in (a)–(d).

The fundamental sensitivity of the hybrid optical pumping SERF atomic magnetometer.

To improve the practicability of the hybrid optical pumping SERF atomic magnetometer, it is necessary for us to investigate the fundamental sensitivity of the magnetometer to improve the sensitivity and stability of the magnetometer and realize the miniaturization of the magnetometer. The fundamental, shot-noise-limited sensitivity of an atomic magnetometer is given by ref. 37

$$\delta B = \frac{1}{\gamma \sqrt{nT_2Vt}}, \tag{7}$$

it is also the ultimate sensibility of the atomic magnetometer[11], where n is the number density of alkali-metal atoms[38], γ is their gyromagnetic ratio and the effective γ for sensitivity estimates is $\gamma = \frac{g\mu_B}{\hbar}$ (equation (7) of ref. 11) in our magnetometer operating at zero field, we replace it by electron gyromagnetic ratio $\gamma_e \left(\gamma_e = \frac{g\mu_B}{\hbar}\right)^{5,38}$, g is the electron g-factor, μ_B is the Bohr magneton, V is the measurement volume, t is the measurement time, T_2 is the transverse spin relaxation time[8], $\frac{1}{T_2} = R_{SD} + R_{wall} + R_{SE}^{ee}$. For the transverse spin relaxation time of the hybrid optical pumping SERF atomic magnetometer, we need consider the spin destruction relaxation R_{SD} caused by He, N$_2$, alkali metal atom A and B, the relaxation rates due to diffusion of alkali metal atoms A and B to the wall[6] R_{wall}^A and R_{wall}^B, the relaxation rate due to alkali-alkali spin-exchange collisions[39] R_{SE}^{ee}, $R_{SE}^{ee} = R_{SE}^{AA} + R_{SE}^{AB} + R_{SE}^{BA} + R_{SE}^{BB}$, which cannot be ignored for large external magnetic field B and is negligible in SERF regime (when T is higher than 418.3 K, B is smaller than 10^{-10} T, $R_{SE}^{ee} \approx 0$), the pumping rate of pump beam R_p and the pumping rate of atom B R_B (R_B is a function of R_p), buffer gas is ^{4}He, quench gas is N$_2$, therefore, $\frac{1}{T_2} = R_{SD}^A + R_{SD}^B + R_{wall}^A + R_{wall}^B + R_{SE}^{AA} + R_{SE}^{AB} + R_{SE}^{BA} + R_{SE}^{BB} + R_p + R_B$, we substitute this term into equation (7) and obtain

$$\delta B = \frac{\sqrt{R_{SD}^A + R_{SD}^B + R_{wall}^A + R_{wall}^B + R_{SE}^{AA} + R_{SE}^{AB} + R_{SE}^{BA} + R_{SE}^{BB} + R_p + R_B}}{\gamma_e \sqrt{nVt}}. \tag{8}$$

However, because alkali metal atom B is probed atom, only these items associated with atom B will be considered in the experiments, we don't consider those items irrelevant to atom B and acquire the fundamental sensitivity of the hybrid optical pumping SERF atomic magnetometer due to the shot-noise as following

$$\delta B' = \frac{\sqrt{R_{wall}^B + R_{SD} + R_B + R_{SE}^{BB} + R_{SE}^{AB} + R_{SE}^{BA}}}{\gamma_e \sqrt{n_B Vt}}. \tag{9}$$

where $R_{wall} = q(P)D_{buffer}^{alkali}\left(\frac{\sqrt{1 + T/273.15}}{P_{buffer}/1amg}\right)\left(\frac{\pi}{a}\right)^2 + q(P)D_{quench}^{alkali}\left(\frac{\sqrt{1 + T/273.15}}{P_{quench}/1amg}\right)\left(\frac{\pi}{a}\right)^2$, the second term that alkali-metal atoms diffuse in the quench gas sometimes is ignored in the experiment, but we find that the harmonic mean of the diffusion coefficients in He and N$_2$ are used for D (diffusion constant of the alkali atom within the gas) in the calculations of ref. 22, hence we also consider the second term, $R_{wall}^B = R_{wall}^{B-He} + R_{wall}^{B-N2}$. $q(P)$ is the nuclear slowing-down factor of alkali-metal atom[40], $q(P)_K = \frac{6 + 2P^2}{1 + P^2}$ for ^{39}K atom, $q(P)_{Rb} = \frac{38 + 52P^2 + 6P^4}{3 + 10P^2 + 3P^4}$ for ^{85}Rb atom, $q(P)_{Cs} = \frac{22 + 70P^2 + 34P^4 + 2P^6}{1 + 7P^2 + 7P^4 + P^6}$ for ^{133}Cs atom, D_{buffer}^{alkali} is the diffusion constant of the alkali atom within the buffer gas[41–43] in units of cm^2/s and is given at 1 amg and 273 K, D_{quench}^{alkali} is the diffusion constant of the alkali atom within the quench gas[42–44] in units of cm^2/s and is given at 1 amg and 273 K, $1 amg = 2.69 \times 10^{19}$ cm^{-3}, $D_{He}^K = 0.35$ cm^2/s, $D_{He}^{Rb} = 0.5$ cm^2/s, $D_{He}^{Cs} = 0.29$ cm^2/s, $D_{N2}^K = 0.2$ cm^2/s, $D_{N2}^{Rb} = 0.19$ cm^2/s, $D_{N2}^{Cs} = 0.098$ cm^2/s, P_{buffer} is the pressure intensity of buffer gas in amg, P_{quench} is the pressure intensity of quench gas in amg, a is the equivalent radius of vapor cell, $R_{SD} = n_{He}\sigma_{SD}^{B-He}\overline{v}_{B-He} + n_{N_2}\sigma_{SD}^{B-N_2}\overline{v}_{B-N_2} + n_B\sigma_{SD}^{B-B}\overline{v}_{B-B} + n_B\sigma_{SD}^{B-A}\overline{v}_{B-A} + n_A\sigma_{SD}^{A-B}\overline{v}_{A-B}$, $R_{SE}^{BB} = \left(\frac{g\mu_B B}{q(0)_B \hbar}\right)^2 \frac{q(0)_B^2 - (2I_B + 1)^2}{2k_{SE}^{B-B}n_B}$, B is the external magnetic field, $q(0)$ is the low polarization limit of the slowing-down factor, I is nuclear spin of the alkali-metal atoms, for ^{39}K, ^{85}Rb and ^{133}Cs, $I_K = 1.5$, $I_{Rb} = 2.5$, $I_{Cs} = 3.5$, the relaxation rate due to alkali-alkali spin-exchange collisions $R_{SE}^{BB} = \left(\frac{g\mu_B B}{q(0)_B \hbar}\right)^2 \frac{q(0)_B^2 - (2I_B + 1)^2}{2k_{SE}^{B-B}n_B}$, $R_{SE}^{BA} = \left(\frac{g\mu_B B}{q(0)_A \hbar}\right)^2 \frac{q(0)_A^2 - (2I_A + 1)^2}{2k_{SE}^{B-A}n_A}$,

$R_{SE}^{AB} = \left(\frac{g\mu_B B}{q(0)_B \hbar}\right)^2 \frac{q(0)_B^2 - (2I_B + 1)^2}{2k_{SE}^{A-B} n_B}$. With sufficiently high alkali metal number density (at higher temperature) and in sufficiently low magnetic field, $R_{SE}^{BB} \approx R_{SE}^{BA} \approx R_{SE}^{AB} \approx 0$. The spin precession rate is $\omega_0 = \frac{g\mu_B B}{q(0)\hbar}$.

Spin-exchange collisions preserve total angular momentum of a colliding pair of atoms but can scramble the hyperfine state of the atoms. Atoms in different hyperfine states do not precess coherently and thereby limit the coherence lifetime of the atoms. However, decoherence due to spin-exchange collisions can be nearly eliminated if the spin-exchange collisions occur much faster than the precession frequency of the atoms. In this regime of fast spin-exchange, all atoms in an ensemble rapidly change hyperfine states, spending the same amounts of time in each hyperfine state and causing the spin ensemble to precess more slowly but remain coherent[13]. In the limit of fast spin-exchange and small magnetic field, the spin-exchange relaxation rate vanishes for sufficiently small magnetic field[11]. In equation (9), we can find that the fundamental sensitivity of the hybrid optical pumping SERF atomic magnetometer increases when part or all of R_{wall}^B, R_{SD}, R_B, R_{SE}^{BB}, R_{SE}^{AB} and R_{SE}^{BA} (the later three terms are approximately zero in sufficiently low magnetic field and the magnetometer is in the SERF regime, which is helpful for us to study how B influence the SERF regime and fundamental sensitivity of the magnetometer) decrease, n_B, V and t increase. For the expressions of R_{wall}^B, R_{SD}, R_B, R_{SE}^{BB}, R_{SE}^{AB}, R_{SE}^{BA}, n_B, V and t, we just need to consider the fundamental sensitivity of the magnetometer change with one of the cell effective radius a, n_{He}, n_{N2}, t, cell temperature T, pumping rate of pump beam (R_p^K and R_p^{Cs}), external magnetic field B and measurement volume V. Diffusion of alkali metal atoms A and B to the wall will corrode the vapor cell and decrease the fundamental sensitivity of the magnetometer. Sufficiently many buffer gas will reduce diffusion of alkali metal atoms A and B to the wall. The probed alkali-metal atoms have a large absorption effect on the pumping beam, it's an additional relaxation item for the alkali-metal atoms of the hybrid optical pumping SERF magnetometer. The spin exchange rate between alkali metal atoms A and alkali metal atoms B play a similar "pumping beam" action. Atom B is polarized by the spin exchange collisions between alkali metal atoms A and B. The pumping effect of probe beam means circularly polarized light in the probe beam pumps alkali-metal atoms. The outer electrons of the alkali metal atoms are polarized by the pumping beam, the polarized electrons undergo Larmor precession under the external magnetic field.

If we consider the influence of the light shift noise[5, 45] B_{LS}, photon shot noise[8] B_{psn}, spin-projection noise[5] B_{spn}, magnetic field noise[46, 47] B_{mag}, technology noise B_{tech} and other noise B_{other} on the SERF atomic magnetometer. Using the method of superposition of power spectral density, we can obtain the sensitivity of the hybrid optical pumping SERF atomic magnetometer as following

$$Sen = \sqrt{(\delta B)^2 + B_{LS}^2 + B_{psn}^2 + B_{spn}^2 + B_{mag}^2 + B_{tech}^2 + B_{other}^2}. \tag{10}$$

If the noises above are optimized by technology means, the sensitivity of the hybrid optical pumping SERF atomic magnetometer approaches to the ultimate sensitivity, which is also helpful to study the atomic spin gyroscope[48–52].

We take one of the cell effective radius a, n_{He}, n_{N2}, t, cell temperature T, pumping rate of pump beam (R_p^K and R_p^{Cs}), B (it is helpful for us to study how B influence the SERF regime and fundamental sensitivity of the magnetometer) and measurement volume V in equation (9) as a variable (other parameters are invariable) to obtain the results that the fundamental sensitivity of the hybrid optical pumping SERF magnetometer based ^{39}K-^{85}Rb-^{4}He and ^{133}Cs-^{85}Rb-^{4}He vary with the variable. Depending on suggestions and the typical conditions of the experiment group[19, 30, 36], in order to facilitate the theoretical analysis, we take the mole fraction of ^{85}Rb $f_{Rb} = 0.97$, $n_{He} = 10^{19} \, cm^{-3}$, $n_{N2} = 2 \times 10^{17} \, cm^{-3}$, $T = 457.5 \, K$, $R_p^K = R_p^{Cs} = 200000 \, s^{-1}$, $a = 1 \, cm$, $V = 1 \, cm^3$, $t = 100 \, s$, $B = 10^{-15} \, T$ ($R_{SE}^{ee} \approx 0$). Because n_K, n_{Rb} and n_{Cs} vary with T, the relation between the fundamental sensitivity of ^{39}K (^{133}Cs)-^{85}Rb-^{4}He magnetometers and the number density of alkali-metal atoms (n_K, n_{Rb} or n_{Cs}) is nonlinear. At the same T (the mole fraction of ^{85}Rb f_{Rb} is fixed), n_K, n_{Rb} and n_{Cs} are different, the fundamental sensitivity are also different. We will study the vapor cell by the characteristics and properties of the microcavities[53–55] in the future work.

Figure 3 shows the relaxation rates due to diffusion of ^{85}Rb in the ^{4}He gas to the wall of ^{39}K-^{85}Rb-^{4}He magnetometer $R_{wall-K-Rb-He}^{Rb-He}$, the total relaxation rates due to diffusion of ^{85}Rb in the ^{4}He and N$_2$ gas to the wall of ^{39}K-^{85}Rb-^{4}He magnetometer $R_{wall-K-Rb-He}^{Rb-He-N2}$, the relaxation rates due to diffusion of ^{85}Rb in the ^{4}He gas to the wall of ^{133}Cs-^{85}Rb-^{4}He magnetometer $R_{wall-Cs-Rb-He}^{Rb-He}$ and the total relaxation rates due to diffusion of ^{85}Rb in the ^{4}He and N$_2$ gas to the wall of ^{133}Cs -^{85}Rb-^{4}He magnetometer $R_{wall-Cs-Rb-He}^{Rb-He-N2}$ decrease when ^{4}He atom number density n_{He} increases, the relaxation rates due to diffusion of ^{85}Rb in the N$_2$ gas to the wall of ^{39}K-^{85}Rb-^{4}He magnetometer $R_{wall-K-Rb-He}^{Rb-N2}$ and the relaxation rates due to diffusion of ^{85}Rb in the N$_2$ gas to the wall of ^{133}Cs-^{85}Rb-^{4}He magnetometer $R_{wall-Cs-Rb-He}^{Rb-N2}$ increase slowly when n_{He} increases in Fig. 3(a). $R_{wall-K-Rb-He}^{Rb-N2}$, $R_{wall-K-Rb-He}^{Rb-He-N2}$, $R_{wall-Cs-Rb-He}^{Rb-N2}$ and $R_{wall-Cs-Rb-He}^{Rb-He-N2}$ decrease when n_{N2} increases, $R_{wall-K-Rb-He}^{Rb-He}$ and $R_{wall-Cs-Rb-He}^{Rb-He}$ increase slowly when n_{N2} increases in Fig. 3(b). $R_{wall-K-Rb-He}^{Rb-He}$, $R_{wall-K-Rb-He}^{Rb-N2}$, $R_{wall-K-Rb-He}^{Rb-He-N2}$, $R_{wall-Cs-Rb-He}^{Rb-He}$, $R_{wall-Cs-Rb-He}^{Rb-N2}$ and $R_{wall-Cs-Rb-He}^{Rb-He-N2}$ decreases slowly when pumping rate of pump beam increases in Fig. 3(c). $R_{wall-K-Rb-He}^{Rb-He}$, $R_{wall-K-Rb-He}^{Rb-He-N2}$, $R_{wall-Cs-Rb-He}^{Rb-He}$ and $R_{wall-Cs-Rb-He}^{Rb-N2}$ increase, $R_{wall-K-Rb-He}^{Rb-He}$ and $R_{wall-Cs-Rb-He}^{Rb-He}$ increase slowly when cell temperature increases in Fig. 3(d). $R_{wall-K-Rb-He}^{Rb-He}$, $R_{wall-K-Rb-He}^{Rb-N2}$, $R_{wall-K-Rb-He}^{Rb-He-N2}$, $R_{wall-Cs-Rb-He}^{Rb-He}$, $R_{wall-Cs-Rb-He}^{Rb-N2}$ and $R_{wall-Cs-Rb-He}^{Rb-He-N2}$ decreases rapidly when the cell effective radius increases in Fig. 3(e). The R_{wall} of ^{39}K-^{85}Rb-^{4}He magnetometer is bigger than the one of ^{133}Cs-^{85}Rb-^{4}He magnetometer.

Figures 4 and 5 show the fundamental sensitivity of ^{39}K (^{133}Cs)-^{85}Rb-^{4}He magnetometers as a function of ^{39}K, ^{133}Cs, ^{85}Rb, ^{4}He and N$_2$ number density, R_p^K and R_p^{Cs}, external magnetic field, cell temperature and measurement
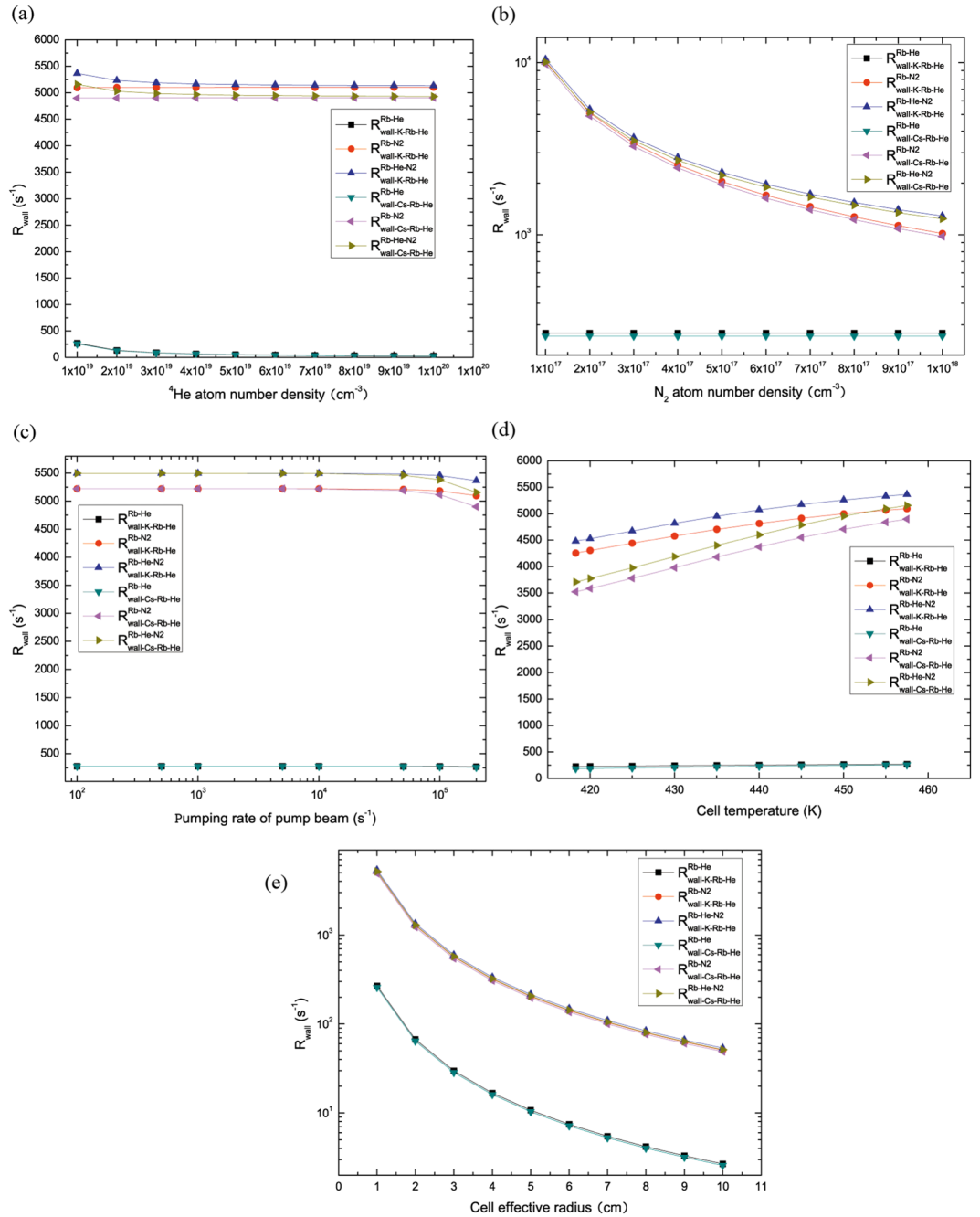
Figure 3. The R_{wall} of ^{39}K-^{85}Rb-^{4}He and ^{133}Cs-^{85}Rb-^{4}He magnetometers vary with the number density of buffer gas ^{4}He and quench gas N$_2$, pumping rate of pump beam, cell temperature and cell effective radius. (**a**) $R_{wall-K-Rb-He}^{Rb-He}$, $R_{wall-K-Rb-He}^{Rb-He-N2}$, $R_{wall-Cs-Rb-He}^{Rb-He}$ and $R_{wall-Cs-Rb-He}^{Rb-He-N2}$ decrease when ^{4}He atom number density n_{He} increases, $R_{wall-K-Rb-He}^{Rb-N2}$ and $R_{wall-Cs-Rb-He}^{Rb-N2}$ increase slowly with increasing ^{4}He atom number density. (**b**) $R_{wall-K-Rb-He}^{Rb-N2}$, $R_{wall-K-Rb-He}^{Rb-He-N2}$, $R_{wall-Cs-Rb-He}^{Rb-N2}$ and $R_{wall-Cs-Rb-He}^{Rb-He-N2}$ decrease as n_{N2} increases, $R_{wall-K-Rb-He}^{Rb-He}$ and $R_{wall-Cs-Rb-He}^{Rb-He}$ increase slowly when n_{N2} increases. (**c**) $R_{wall-K-Rb-He}^{Rb-He}$, $R_{wall-K-Rb-He}^{Rb-N2}$, $R_{wall-K-Rb-He}^{Rb-He-N2}$, $R_{wall-Cs-Rb-He}^{Rb-He}$, $R_{wall-Cs-Rb-He}^{Rb-N2}$ and $R_{wall-Cs-Rb-He}^{Rb-He-N2}$ decreases slowly when pumping rate of pump beam increases. (**d**) $R_{wall-K-Rb-He}^{Rb-N2}$, $R_{wall-K-Rb-He}^{Rb-He-N2}$, $R_{wall-Cs-Rb-He}^{Rb-N2}$ and $R_{wall-Cs-Rb-He}^{Rb-He-N2}$ increase rapidly, $R_{wall-K-Rb-He}^{Rb-He}$ and $R_{wall-Cs-Rb-He}^{Rb-He}$ increase slowly when T increases. (**e**) $R_{wall-K-Rb-He}^{Rb-He}$, $R_{wall-K-Rb-He}^{Rb-N2}$, $R_{wall-K-Rb-He}^{Rb-He-N2}$, $R_{wall-Cs-Rb-He}^{Rb-He}$, $R_{wall-Cs-Rb-He}^{Rb-N2}$ and $R_{wall-Cs-Rb-He}^{Rb-He-N2}$ decreases rapidly when the cell effective radius increases. The R_{wall} of ^{39}K-^{85}Rb-^{4}He magnetometer is bigger than the one of ^{133}Cs-^{85}Rb-^{4}He magnetometer.
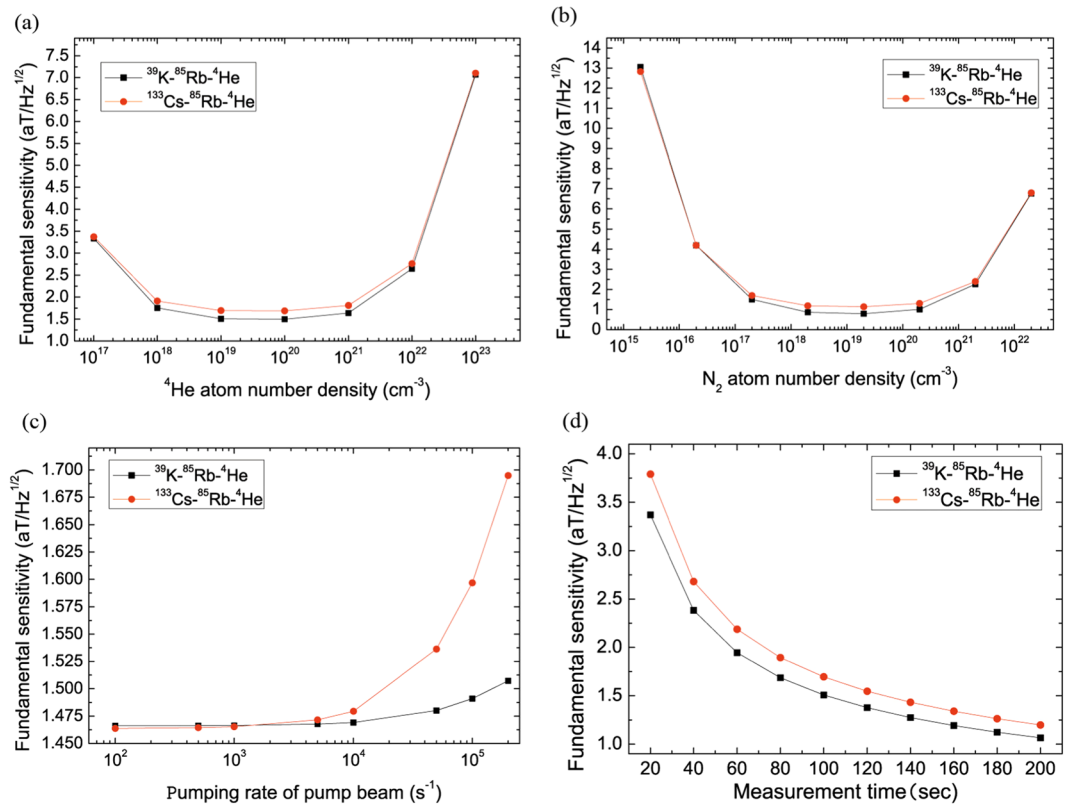
Figure 4. The fundamental sensitivity of ^{39}K (^{133}Cs)-^{85}Rb-^4He magnetometers varies with the number density of buffer gas ^4He and quench gas N_2, pumping rate of pump beam, measurement time. (**a**) The fundamental sensitivity of ^{39}K-^{85}Rb-^4He magnetometer (black line in squares) increases with the increasing number density of ^4He when ^4He number density is smaller than a critical value about $4.22 \times 10^{19}\, cm^{-3}$ and decreases when ^4He number density is bigger than the value. The fundamental sensitivity of ^{133}Cs-^{85}Rb-^4He magnetometer (red line in dots) increases with the increasing number density of ^4He when ^4He number density is smaller than a critical value about $4.15 \times 10^{19}\, cm^{-3}$ and decreases when ^4He number density is bigger than the value. (**b**) The fundamental sensitivity of ^{39}K-^{85}Rb-^4He magnetometer (black line in squares) increases with the increasing N_2 number density when N_2 number density is smaller than a critical value about $1.22 \times 10^{19}\, cm^{-3}$ and decreases when N_2 number density is higher than the value. The fundamental sensitivity of ^{133}Cs-^{85}Rb-^4He magnetometer(red line in dots) increases with the increasing N_2 number density when N_2 number density is smaller than a critical value about $1.21 \times 10^{19}\, cm^{-3}$ and decreases when N_2 number density is higher than the value. The fundamental sensitivity of ^{39}K (^{133}Cs)-^{85}Rb-^4He magnetometers decrease with the increasing pumping rate of pump beam in (**c**). The fundamental sensitivity of ^{39}K (^{133}Cs)-^{85}Rb-^4He magnetometers increase with the increasing measurement time. The fundamental sensitivity of ^{133}Cs-^{85}Rb-^4He magnetometer is lower than the one of ^{39}K-^{85}Rb-^4He magnetometer in (**d**).

time, cell effective radius, measurement volume, includes the effects of spin exchange due to ^{39}K-^{85}Rb, ^{85}Rb-^{85}Rb, ^{85}Rb-^{39}K, ^{133}Cs-^{85}Rb, ^{85}Rb-^{133}Cs and spin relaxation due to ^{39}K-^{85}Rb, ^{85}Rb-^{85}Rb, ^{85}Rb-^{39}K, ^{133}Cs-^{85}Rb, ^{85}Rb-^{133}Cs, ^{85}Rb-^4He collisions, ^{85}Rb-N_2 destructions.

Figure 4(a) represents that the fundamental sensitivity of ^{39}K-^{85}Rb-^4He magnetometer (black line in squares) increases with the increasing ^4He number density when ^4He number density is smaller than a critical value about $4.22 \times 10^{19}\, cm^{-3}$, it decreases when ^4He number density is higher than the value. The fundamental sensitivity of ^{133}Cs-^{85}Rb-^4He magnetometer (red line in dots) increases with the increasing ^4He number density when ^4He number density is smaller than a critical value about $4.15 \times 10^{19}\, cm^{-3}$ and it decreases when ^4He number density is higher than the value. For this phenomenon, we think that more alkali-metal atoms diffuse to the cell wall and less spin exchange collisions between alkali-metal atoms A and B when ^4He number density is smaller than the value and decrease. Less alkali-metal atoms diffuse to the cell wall and more spin exchange collisions between alkali-metal atoms and buffer gas so that there are less spin exchange collisions in alkali-metal atoms when the number density of ^4He is bigger than the value and increase. Therefore, if we take the critical value as ^4He number density, spin exchange collisions in alkali-metal atoms are the most, we can obtain the highest fundamental sensitivity of the magnetometer.

Figure 4(b) shows that the fundamental sensitivity of ^{39}K-^{85}Rb-^4He magnetometer (black line in squares) increases with the increasing N_2 number density when N_2 number density is smaller than a critical value about $1.22 \times 10^{19}\, cm^{-3}$, it decreases when N_2 number density is higher than the value. The fundamental sensitivity of ^{133}Cs-^{85}Rb-^4He magnetometer (red line in dots) increases with the increasing N_2 number density when N_2
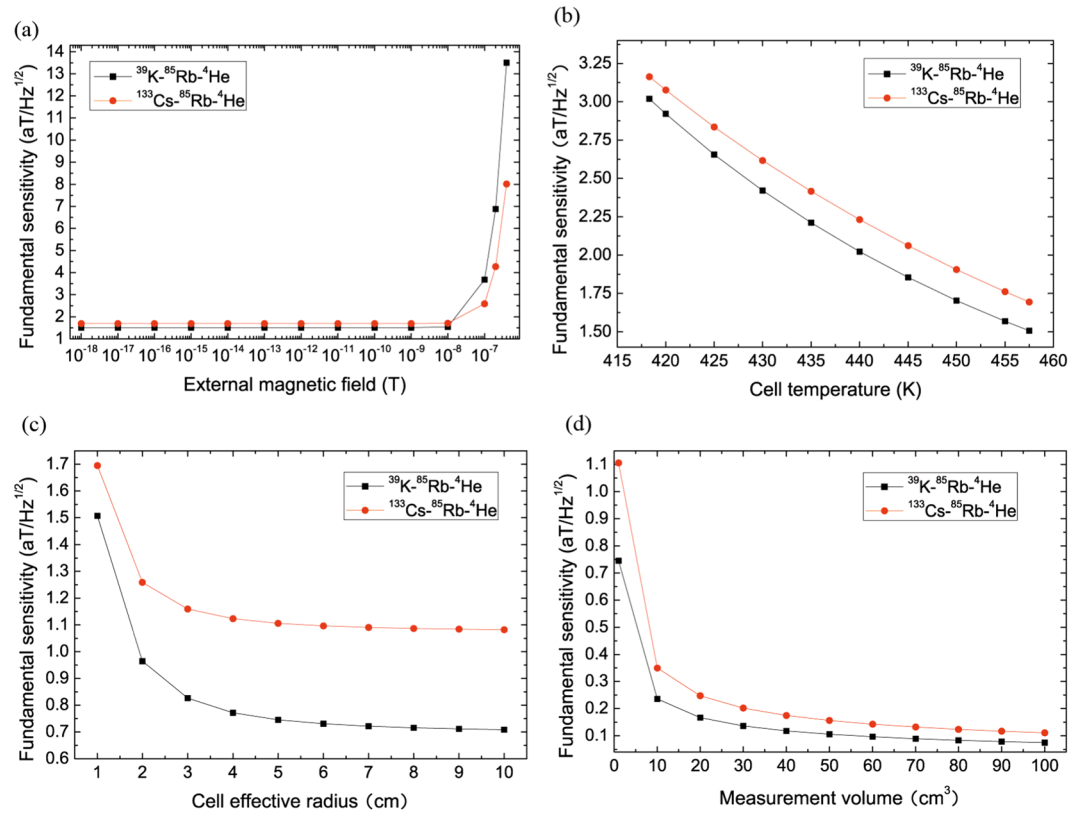
Figure 5. The fundamental sensitivity of ^{39}K (^{133}Cs)-^{85}Rb-^{4}He magnetometers varies with the external magnetic field, cell temperature, cell effective radius and measurement volume. (**a**) When the external magnetic field is smaller than about 10^{-8} T, the fundamental sensitivity of ^{39}K (^{133}Cs)-^{85}Rb-^{4}He magnetometers almost do not vary with the increasing external magnetic field respectively. (**b**) The fundamental sensitivity of ^{39}K (^{133}Cs)-^{85}Rb-^{4}He magnetometers increase with the increasing cell temperature respectively. (**c**) The fundamental sensitivity of ^{39}K (^{133}Cs)-^{85}Rb-^{4}He magnetometers increase with the increasing cell effective radius respectively. (**d**) The fundamental sensitivity of ^{39}K (^{133}Cs)-^{85}Rb-^{4}He magnetometers with $a = 5\,cm$ increase with increasing measurement volume respectively.

number density is smaller than a critical value about $1.21 \times 10^{19}\,cm^{-3}$, it decreases when N$_2$ number density is higher than the value. Therefore, if we take the critical value as N$_2$ number density, we can obtain the highest fundamental sensitivity of the magnetometer. The fundamental sensitivity of ^{39}K (^{133}Cs)-^{85}Rb-^{4}He magnetometers decrease with the increasing pumping rate of pump beam respectively in Fig. 4(c). When the pumping rate of pump beam is bigger than about $1916\,s^{-1}$ and N$_2$ number density is bigger than about $1.974 \times 10^{16}\,cm^{-3}$, the fundamental sensitivity of ^{39}K-^{85}Rb-^{4}He magnetometer is higher than the one of ^{133}Cs-^{85}Rb-^{4}He magnetometer. The fundamental sensitivity of ^{39}K (^{133}Cs)-^{85}Rb-^{4}He magnetometers (black line in squares and red line in dots) increase with the increasing measurement time. The fundamental sensitivity of ^{133}Cs-^{85}Rb-^{4}He magnetometer is lower than the one of ^{39}K-^{85}Rb-^{4}He magnetometer in Fig. 4(d).

Figure 5 describes that when the external magnetic field B is smaller than about 10^{-8} T, the fundamental sensitivity of ^{39}K-^{85}Rb-^{4}He magnetometer is higher than the one of ^{133}Cs-^{85}Rb-^{4}He magnetometer and they almost do not vary with the increasing external magnetic field respectively, the fundamental sensitivity decreases rapidly when B is bigger than about 10^{-8} T and the fundamental sensitivity of ^{39}K-^{85}Rb-^{4}He magnetometer is lower than the one of ^{133}Cs-^{85}Rb-^{4}He magnetometer when B is bigger than about 2.845×10^{-8} T in Fig. 5(a). The fundamental sensitivity of ^{39}K (^{133}Cs)-^{85}Rb-^{4}He magnetometers increase with the increasing cell temperature respectively and there are more spin exchange collisions in alkali-metal atoms in Fig. 5(b). The fundamental sensitivity of ^{39}K (^{133}Cs)-^{85}Rb-^{4}He magnetometers increase with the increasing cell effective radius respectively in Fig. 5(c). The fundamental sensitivity of ^{39}K (^{133}Cs)-^{85}Rb-^{4}He magnetometers with $a = 5cm$ increase with increasing measurement volume respectively in Fig. 5(d). The fundamental sensitivity of ^{133}Cs-^{85}Rb-^{4}He magnetometer is lower than the one of ^{39}K-^{85}Rb-^{4}He magnetometer in Fig. 5(a)–(d).

As a result, the polarization of ^{85}Rb atom of the hybrid optical pumping SERF magnetometer based on ^{133}Cs-^{85}Rb-^{4}He is bigger than the one based on ^{39}K-^{85}Rb-^{4}He in Fig. 2. However, the fundamental sensitivity of ^{39}K-^{85}Rb-^{4}He magnetometer is higher than the one of ^{133}Cs-^{85}Rb-^{4}He magnetometer when the pumping rate of pump beam is bigger than about $1916\,s^{-1}$ in figures 4 and 5. For another buffer gas ^{21}Ne, a large ^{85}Rb magnetization field due to spin interaction between ^{85}Rb atom and ^{21}Ne atoms causes a large spin exchange relaxation rate of ^{85}Rb atom[56] and ^{85}Rb atom can make ^{21}Ne atoms hyperpolarized, which will affect the magnetic

parameter	value
Boltzmann's constant k_B	$1.38 \times 10^{-23}\, J/K$
Atomic mass unit m	$1.660539040(20) \times 10^{-27}\, kg$
π	3.14
Electron spin g factor	2×1.001159657
Planck's constant $\hbar$	$1.054589 \times 10^{-34}\, Js$
Bohr magneton μ_B	$9.27408 \times 10^{-24}\, J/T$
$D_0\,(K-He)$[41]	$0.35\, cm^2/s$
$D_0\,(Rb-He)$[42]	$0.5\, cm^2/s$
$D_0\,(Cs-He)$[43]	$0.291\, cm^2/s$
$D_0\,(K-N2)$[44]	$0.2\, cm^2/s$
$D_0\,(Rb-N2)$[42]	$0.19\, cm^2/s$
$D_0\,(Cs-N2)$[43]	$0.098\, cm^2/s$
σ_{SE}^{K}[31]	$1.8 \times 10^{-14}\, cm^2$
σ_{SE}^{Rb}[27]	$1.9 \times 10^{-14}\, cm^2$
σ_{SE}^{Cs}[27]	$2.1 \times 10^{-14}\, cm^2$
σ_{SD}^{K}[32]	$1 \times 10^{-18}\, cm^2$
σ_{SD}^{Rb}[33]	$1.6 \times 10^{-17}\, cm^2$
σ_{SD}^{Cs}[34]	$2 \times 10^{-16}\, cm^2$
σ_{SE}^{K-Rb}	$\sigma_{SE}^{K}\frac{n_K}{n_K+n_{Rb}} + \sigma_{SE}^{Rb}\frac{n_{Rb}}{n_K+n_{Rb}}$
σ_{SE}^{Rb-K}	$\sigma_{SE}^{Rb}\frac{n_{Rb}}{n_K+n_{Rb}} + \sigma_{SE}^{K}\frac{n_K}{n_K+n_{Rb}}$
σ_{SE}^{Cs-Rb}	$\sigma_{SE}^{Cs}\frac{n_{Cs}}{n_{Cs}+n_{Rb}} + \sigma_{SE}^{Rb}\frac{n_{Rb}}{n_{Cs}+n_{Rb}}$
σ_{SE}^{Rb-Cs}	$\sigma_{SE}^{Rb}\frac{n_{Rb}}{n_{Cs}+n_{Rb}} + \sigma_{SE}^{Cs}\frac{n_{Cs}}{n_{Cs}+n_{Rb}}$
$\sigma_{SE}^{{}^{87}Rb-{}^{133}Cs}$[26]	$(2.3 \pm 0.2) \times 10^{-14}\, cm^2$
σ_{SD}^{K-Rb}	$\sigma_{SD}^{K}\frac{n_K}{n_K+n_{Rb}} + \sigma_{SD}^{Rb}\frac{n_{Rb}}{n_K+n_{Rb}}$
σ_{SD}^{Rb-K}	$\sigma_{SD}^{Rb}\frac{n_{Rb}}{n_K+n_{Rb}} + \sigma_{SD}^{K}\frac{n_K}{n_K+n_{Rb}}$
σ_{SD}^{Cs-Rb}	$\sigma_{SD}^{Cs}\frac{n_{Cs}}{n_{Cs}+n_{Rb}} + \sigma_{SD}^{Rb}\frac{n_{Rb}}{n_{Cs}+n_{Rb}}$
σ_{SD}^{Rb-Cs}	$\sigma_{SD}^{Rb}\frac{n_{Rb}}{n_{Cs}+n_{Rb}} + \sigma_{SD}^{Cs}\frac{n_{Cs}}{n_{Cs}+n_{Rb}}$
σ_{SD}^{K-He}[11]	$8 \times 10^{-25}\, cm^2$
σ_{SD}^{Rb-He}[11]	$9 \times 10^{-24}\, cm^2$
σ_{SD}^{Cs-He}[11]	$2.8 \times 10^{-23}\, cm^2$
σ_{SD}^{K-N2}[25, 35]	$7.9 \times 10^{-23}\, cm^2$
σ_{SD}^{Rb-N2}[25, 11]	$1 \times 10^{-22}\, cm^2$
σ_{SD}^{Cs-N2}[25, 11]	$5.5 \times 10^{-22}\, cm^2$
Nuclear Spin of ^{39}K I_K	1.5
Nuclear Spin of ^{85}Rb I_{Rb}	2.5
Nuclear Spin of ^{133}Cs I_{Cs}	3.5

Table 1. Parameters used for the calculation.

field measurement, it is a better choice to take ^{4}He as the buffer gas of the SERF magnetometer to measure the magnetic field and take ^{21}Ne as the buffer gas of the SERF magnetometer to measure inertia. The fundamental sensitivity of the magnetometers based on ^{133}Cs-^{85}Rb-^{4}He is lower than the one based on ^{39}K-^{85}Rb-^{4}He when the pumping rate of pump beam is bigger than about $1916\, s^{-1}$ and B is bigger than about $2.845 \times 10^{-8}\, T$ (the magnetometers are not in the SERF regime for this external magnetic field).

The polarization of ^{85}Rb atom of the magnetometer is uniform when the mole fraction of ^{85}Rb $f_{Rb} = 0.97$, $n_{He} = 10^{19}\, cm^{-3}$, $n_{N2} = 2 \times 10^{17}\, cm^{-3}$, $T = 457.5\, K$, $R_p^K = R_p^{Cs} = 200000\, s^{-1}$, $a = 1\, cm$, $V = 1\, cm^3$, $B = 10^{-15}\, T$ and $t = 100\, s$. Under above condition, we obtain a fundamental sensitivity of $1.5073\, aT/Hz^{1/2}$ with ^{39}K-^{85}Rb-^{4}He magnetometer with ^{85}Rb polarization is 0.1116 and $n_K/n_{Rb} = 0.0023$, a fundamental sensitivity of $1.6949\, aT/Hz^{1/2}$ with ^{133}Cs-^{85}Rb-^{4}He magnetometer with ^{85}Rb polarization is 0.1864 and $n_{Cs}/n_{Rb} = 0.0151$. By optimizing above parameters, we obtain a fundamental sensitivity of $1.8359 \times 10^{-2}\, aT/Hz^{1/2}$ with ^{39}K-^{85}Rb-^{4}He with the polarization of ^{85}Rb atom is 1.3174×10^{-4} and $n_K/n_{Rb} = 0.0023$, a fundamental sensitivity of $1.8181 \times 10^{-2}\, aT/Hz^{1/2}$ with ^{133}Cs-^{85}Rb-^{4}He with the polarization of ^{85}Rb atom is 2.3316×10^{-4} and $n_{Cs}/n_{Rb} = 0.0151$ with the mole fraction of ^{85}Rb $f_{Rb} = 0.97$, $n_{He} = 10^{19}\, cm^{-3}$, $n_{N2} = 2 \times 10^{17}\, cm^{-3}$, $T = 457.5\, K$, $R_p^K = R_p^{Cs} = 200\, s^{-1}$, $a = 10\, cm$, $B = 10^{-15}\, T$, $V = 1000\, cm^3$, $t = 100\, s$, with higher fundamental sensitivity possible at bigger measurement volume, proper amount of buffer gas and quench gas, smaller pumping rate of pump beam, higher temperature and longer measurement time.
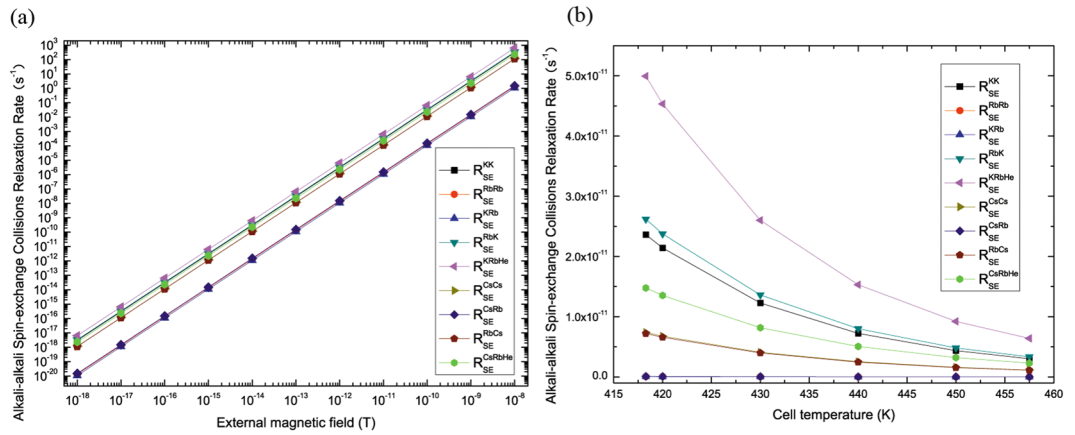
Figure 6. The alkali-alkali spin-exchange collisions relaxation rate of ^{39}K (^{133}Cs)-^{85}Rb-^{4}He magnetometers varies with the external magnetic field and cell temperature. R_{SE}^{KK}, R_{SE}^{RbRb}, R_{SE}^{KRb}, R_{SE}^{RbK} and their total spin-exchange collisions relaxation rate R_{SE}^{KRbHe} increase, R_{SE}^{CsCs}, R_{SE}^{RbRb}, R_{SE}^{CsRb}, R_{SE}^{RbCs} and their total spin-exchange collisions relaxation rate R_{SE}^{CsRbHe} increase when B increases and decrease when T increases in (**a**) and (**b**).

Discussion

In conclusion, we find that ^{85}Rb polarization increases with the increasing pumping rate of pump beam. The ^{85}Rb polarization of ^{133}Cs-^{85}Rb-^{4}He magnetometer is bigger than the one of ^{39}K-^{85}Rb-^{4}He magnetometer. The polarization of ^{85}Rb atom of ^{39}K (^{133}Cs)-^{85}Rb-^{4}He magnetometers almost do not vary when the number density of ^{4}He and N$_2$ increase and the number density of ^{4}He and N$_2$ are smaller than some critical values and decrease rapidly when the number density of buffer gas and quench gas are bigger than the values respectively. The fundamental sensitivity increases with the increasing number density of buffer gas and quench gas when the number density of buffer gas and quench gas are smaller than corresponding critical values respectively and decreases when the number density of buffer gas and quench gas are bigger than the values. The fundamental sensitivity increases with the increasing cell effective radius, measurement volume, cell temperature and measurement time respectively. The fundamental sensitivity of the magnetometers decrease with increasing R_p^K and R_p^{Cs}. At the same cell temperature, the polarization of ^{85}Rb atom of ^{133}Cs-^{85}Rb-^{4}He magnetometer is bigger than the one of ^{39}K-^{85}Rb-^{4}He magnetometer and the fundamental sensitivity of ^{133}Cs-^{85}Rb-^{4}He magnetometer is lower than the one of ^{39}K-^{85}Rb-^{4}He magnetometer when the pumping rate of pump beam is bigger than about 1916 s^{-1} and B is smaller than about 2.845×10^{-8} T.

From the formula of the relative velocity, R_{wall}, R_{SE}^{ee}, n_A, n_B and equation (1), we can find that increasing the cell temperature will increase R_{wall}, R_{SD} and the number density of alkali-metal atoms, reduce R_{SE}^{ee}. In general, R_{SE}^{ee} is smaller than R_{wall} and R_{SD}, raising the cell temperature resulting in an increase in the fundamental sensitivity is mainly due to the great improvement of the probed alkali-metal atomic number density when the cell temperature inceases, which has a greater influence on the fundamental sensitivity than R_{wall} and R_{SD}. If the number density of alkali-metal atoms and cell volume are fixed, in other words, when the alkali-metal atoms in the vapor cell are fully in the vapor regime, if we continue to raise the cell temperature, the alkali-metal atoms number density will not change, R_{SE}^{ee} will decrease, R_{wall} and R_{SD} will increase. What's more, the decreased value of R_{SE}^{ee} is smaller than the increased value of R_{wall} and R_{SD}, which will decrease the fundamental sensitivity. For example, there are certain amount of alkali-metal atoims ^{39}K(^{133}Cs) and ^{85}Rb with the mole fraction of ^{85}Rb is 0.97 in the hybrid vapor cell, when $T = 418.3$ K, all of the alkali-metal atoims become vapor, $n_K = 3.0072 \times 10^{11}$ cm^{-3}, $n_{Rb} = 1.7385 \times 10^{14}$ cm^{-3}, $n_{Cs} = 2.3741 \times 10^{12}$ cm^{-3} with $a = 1$ cm, if we continue to increase T, we will find that n_K, n_{Cs} and n_{Rb} do not change. When $n_{He} = 10^{19}$ cm^{-3}, $n_{N2} = 2 \times 10^{17}$ cm^{-3}, $R_p^K = R_p^{Cs} = 200000 s^{-1}$, $a = 1$ cm, $V = 1$ cm^3, $B = 10^{-15}$ T, $t = 100$ s, the fundamental sensitivity of ^{39}K-^{85}Rb-^{4}He and ^{133}Cs-^{85}Rb-^{4}He magnetometers are 3.0191 $aT/Hz^{1/2}$ and 3.1630 $aT/Hz^{1/2}$ at $T = 418.3$ K, 2.4204 $aT/Hz^{1/2}$ and 2.6163 $aT/Hz^{1/2}$ at $T = 430$ K.

In practical applications, we should consider some questions, one very essential question is the minimum total number of atoms necessary for the operation of the magnetometer with the desired accuracy, as well as the geometric size of the setup - how small can it be made? How does the fundamental sensitivity of the elaborated setup depend on the number of atoms?

Firstly, we can find that when the number density of alkali-metal atom (which is determined by the mole fraction and cell temperature for the hybrid vapor cell with two types of alkali-metal atoms), buffer gas and quench gas are certain, if we also know the effective radius of vapor cell, pumping rate of pump beam, external magnetic field, measurement volume and measurement time, we can obtain the corresponding total number of the atoms and the fundamental sensitivity of the magnetometer. Because the number density of alkali-metal atom is determined by the mole fraction and cell temperature for the hybrid vapor cell with two types of alkali-metal atoms, we can find that how the fundamental sensitivity of the magnetometer depend on the number density of alkali-metal atom, buffer gas and quench gas from Figs 4(a),(b) and 5(b) (the mole fraction and cell temperature corresponds to the number density of alkali metal atoms). The less number density of buffer gas and quench gas, the bigger R_{wall}, it's hard to say the minimum number density of buffer gas and quench gas, but we find that there

are critical values for the number density of buffer gas and quench gas to make the fundamental sensitivity of the magnetometers highest.

Secondly, the smallest geometric size of the setup and volume of vapor cell depends on the processing method and materials. For example, Griffith et al. studied a miniature atomic magnetometer integrated with flux concentrators, the magnetometer uses a millimeter scale ^{87}Rb vapor cell ($3 \times 2 \times 1\ mm^3$) and either mu-metal or Mn-Zn ferrite flux concentrators. They found that the minimum separation of the concentrators is limited to 2 mm by the external dimensions of the vapor cell[57] and reached a sensitivity of $10^4\ aT/Hz^{1/2}$.

Thirdly, if the amount of ^{39}K (^{133}Cs) is little (all of ^{39}K (^{133}Cs) atoms become vapor when $T = 418.3\ K$) and there is enough ^{85}Rb in the vapor cell, when T is bigger than 418.3 K. We continue to increase T, we will find that n_K/n_{Rb} (n_{Cs}/n_{Rb}) gets bigger and bigger, the fundamental sensitivity becomes higher and higher. For instance, Fang et al.[19] obtained a sensitivity of approximately $5 \times 10^3\ aT/Hz^{1/2}$ by optimizing the parameters of SERF magnetometer based on K-Rb hybrid optical pumping when the mole fraction of K atoms is approximately 0.03. Ito et al. studied optimal densities of alkali metal atoms in an optically pumped K-Rb hybrid atomic magnetometer considering the spatial distribution of spin polarization, calculated the spatial distribution of the spin polarization and found that the optimal density of K atoms is $3 \times 10^{13}\ cm^{-3}$ and the optimal density ratio is $n_K/n_{Rb} \sim 400$ (Rb as pump atoms and K as probe atoms) to maximize the output signal and enhance spatial homogeneity of the sensor property[22].

Fourthly, the alkali-metal atoms in the vapor cell are operated in the "hot-gas" regime. If the atomic gas is cooled to the state of a Bose-Einstein condensation (BEC), the operation may be essentially improved. For example, Wildermuth et al. experimentally sensed electric and magnetic fields with BEC and found this field sensor simultaneously features high spatial resolution and high field sensitivity, reached a sensitivity of $\sim 10^9\ aT$ at 3 μm spatial resolution[58]. Therefore, we can use BEC magnetometer to obtain higher sensitivity of magnetic field and spatial resolution, which is very important for the application of the magnetometer in the field of biomedicine.

If we take $\sigma_{SD}^{K-Rb} = \sigma_{SD}^{Rb-K} \approx \sigma_{SD}^{Rb} = 1.6 \times 10^{-17}\ cm^2$, $\sigma_{SD}^{Cs-Rb} = \sigma_{SD}^{Rb-Cs} \approx \sigma_{SD}^{Cs} = 2 \times 10^{-16}\ cm^2$, the polarization and fundamental sensitivity of the magnetometer will decrease slightly, but it will not affect the change rule of the polarization and fundamental sensitivity discussed above. To obtain a higher fundamental sensitivity between ^{39}K-^{85}Rb-^{4}He and ^{133}Cs-^{85}Rb-^{4}He magnetometers, it is better to choose ^{39}K-^{85}Rb-^{4}He magnetometer (when the pumping rate of pump beam is bigger than about 1916 s^{-1}, N$_2$ number density is bigger than about $1.974 \times 10^{16}\ cm^{-3}$ and B is smaller than about $2.845 \times 10^{-8}\ T$), with ^{4}He as the buffer gas and take the critical value of ^{4}He number density and quench gas, increase a, V, T (when the quantity of alkali-metal atoms are enough), t, then reduce B and the pumping rate of pump beam based on actual demand of the fundamental sensitivity and spatial resolution. We estimate the fundamental sensitivity limit of the hybrid optical pumping SERF magnetometer due to the shot-noise superior to $1.8359 \times 10^{-2}\ aT/Hz^{1/2}$, which is higher than the shot-noise-limited sensitivity of 1 $aT/Hz^{1/2}$ of K SERF atomic magnetometer. We could choose suitable conditions on the basis of the experiment requirements to gain a higher sensitivity of the SERF magnetometer, keep the costs down and carry forward the miniaturization and practical application of the hybrid optical pumping SERF atomic magnetometers. The influences of the mole fraction of ^{85}Rb f_{Rb} as a variable on the polarization and fundamental sensitivity of the hybrid optical pumping SERF atomic magnetometer will be investigated in the future work.

Methods

The fundamental sensitivity calculation details. We obtain the above calculation results by MATLAB and chose some special points to plot with Origin 8. The fundamental sensitivity of the hybrid optical pumping SERF atomic magnetometer was obtained by equation (9) and relevant parameters used listed in Table 1 and taking one of the cell effective radius a, n_{He}, n_{N2}, measurement time t, cell temperature T, pumping rate of pump beam (R_p^K and R_p^{Cs}), external magnetic field B and measurement volume V by equation (9) as a variable (other parameters are invariable) and the fundamental sensitivity of ^{39}K-^{85}Rb-^{4}He and ^{133}Cs-^{85}Rb-^{4}He magnetometer vary with the variable in Figs 4(a)–(d) and 5(a)–(d), where the mole fraction of ^{85}Rb $f_{Rb} = 0.97$, $n_{He} = 10^{19}\ cm^{-3}$, $n_{N2} = 2 \times 10^{17}\ cm^{-3}$, $T = 457.5\ K$, $R_p^K = R_p^{Cs} = 200000\ s^{-1}$, $a = 1\ cm$, $V = 1\ cm^3$, $t = 100\ s$, $B = 10^{-15}\ T$ and the magnetometer polarization is obtained by equation (6) and its relevant parameters are chosen as above. For R_{SE}^{KK}, R_{SE}^{RbRb}, R_{SE}^{KRb}, R_{SE}^{RbK} and their total spin-exchange collisions relaxation rate R_{SE}^{KRbHe} increase, R_{SE}^{CsCs}, R_{SE}^{RbRb}, R_{SE}^{CsRb}, R_{SE}^{RbCs} and their total spin-exchange collisions relaxation rate R_{SE}^{CsRbHe} increase when B increases and decrease when T increases in Fig. 6. We find that $R_{SE}^{AA}\left(R_{SE}^{AA} = \left(\frac{g\mu_B B}{q(0)_A \hbar}\right)^2 \frac{q(0)_A^2 - (2I_A + 1)^2}{2k_{SE}^{A-A} n_A}\right)$, R_{SE}^{BB}, R_{SE}^{AB}, R_{SE}^{BA} and R_{SE}^{ee} ($R_{SE}^{ee} = R_{SE}^{AA} + R_{SE}^{BB} + R_{SE}^{AB} + R_{SE}^{BA}$) increase when B increases and decrease when T increases. When T is higher than 418.3 K, B is smaller than $10^{-10}\ T$, $R_{SE}^{ee} \approx 0$. When B is bigger than $10^{-9}\ T$ and T is lower than 400 K, we can not ignore the effect of the alkali-alkali spin-exchange collisions relaxation rate. Therefore, there need to reduce the external magnetic field to $10^{-10}\ T$ below and make the cell temperature higher than 418.3 K to reduce the effect of alkali-alkali spin-exchange collisions relaxation rate on the SERF regime and weak magnetic field measurement in the experiments.

References

1. Johnson, C. N., Schwindt, P. D. D. & Weisend, M. Multi-sensor magnetoencephalography with atomic magnetometers. *Phys. Med. Biol.* **58**, 6065–6077 (2013).
2. Sander, T. H. et al. Magnetoencephalography with a chip-scale atomic magnetometer. *Biomed. Opt. Express* **3**, 981–990 (2012).
3. Wyllie, R., Kauer, M., Smetana, G. S., Wakai, R. T. & Walker, T. G. Magnetocardiography with a modular spin-exchange relaxation free atomic magnetometer array. *Phys. Med. Biol.* **57**, 2619–2632 (2012).
4. Brown, J. M., Smullin, S. J., Kornack, T. W. & Romalis, M. V. New Limit on Lorentz- and CPT-Violating Neutron Spin Interactions. *Phys. Rev. Lett.* **105**, 151604 (2010).
5. Seltzer, S. J. Developments in Alkali-Metal Atomic Magnetometry. *Princeton University* (2008).

6. Kornack, T. W. A Test of CPT and Lorentz Symmetry Using a K-^{3}He Co-magnetometer. *Princeton University* (2005).
7. Fang, J. C., Qin, J., Wan, S. A., Chen, Y. & Li, R. J. Atomic spin gyroscope based on ^{129}Xe-Cs comagnetometer. *Chin. Sci. Bull.* **58**, 1512–1515 (2013).
8. Ledbetter, M. P., Savukov, I. M., Acosta, V. M., Budker, D. & Romalis, M. V. Spin-exchange-relaxation-free magnetometry with Cs vapor. *Phys. Rev. A* **77**, 033408 (2008).
9. Nelson, I. A. Physics of Practical Spin-Exchange Optical Pumping. *University of Wisconsin - Madison* (2001).
10. Kominis, I. K., Kornack, T. W., Allred, J. C. & Romalis, M. V. A subfemtotesla multichannel atomic magnetometer. *Nature* **422**, 596–599 (2003).
11. Allred, J. C., Lyman, R. N., Kornack, T. W. & Romalis, M. V. High-sensitivity atomic magnetometer unaffected by spin-exchange relaxation. *Phys. Rev. Lett.* **89**, 130801 (2002).
12. Happer, W. & Tang, H. Spin-exchange shift and narrowing of magnetic resonance lines in optically pumped alkali vapors. *Phys. Rev. Lett.* **31**, 273–276 (1973).
13. Happer, W. & Tam, A. C. Effect of rapid spin exchange on the magnetic-resonance spectrum of alkali vapors. *Phys. Rev. A* **16**, 1877–1891 (1977).
14. Dong, H. F., Xuan, L. F., Zhuo, C. & Lin, H. B. Two Unshielded SERF Magnetometer Schemes and Their Comparison. *J. Test Meas. Techol.* **26**, 468 (2012).
15. Ito, Y., Ohnishi, H., Kamada, K. & Kobayashi, T. Effect of spatial homogeneity of spin polarization on magnetic field response of an optically pumped atomic magnetometer using a hybrid cell of K and Rb atoms. *IEEE T. Magn.* **48**, 3715–3718 (2012).
16. Romalis, M. V. Hybrid optical pumping of optically dense alkali-metal vapor without quenching gas. *Phys. Rev. Lett.* **105**, 243001 (2010).
17. Ito, Y., Ohnishi, H., Kamada, K. & Kobayashi, T. Sensitivity Improvement of Spin-Exchange Relaxation Free Atomic Magnetometers by Hybrid Optical Pumping of Potassium and Rubidium. *IEEE T. Magn.* **47**, 3550–3553 (2011).
18. Ito, Y., Ohnishi, H., Kamada, K. & Kobayashi, T. Rate-equation Approach to Optimal Density Ratio of K-Rb Hybrid Cell for Optically Pumped Atomic Magnetometers. *35th Annual International Conference of the IEEE EMBS* **6**, 3254–3257 (2013).
19. Fang, J. C., Wang, T., Zhang, H., Li, Y. & Zou, S. Optimizations of spin-exchange relaxation-free magnetometer based on potassium and rubidium hybrid optical pumping. *Rev. Sci. Instrum.* **85**, 123104 (2014).
20. Li, Y., Cai, H. W., Ding, M., Quan, W. & Fang, J. C. A Subfemtotesla Atomic Magnetometer Based on Hybrid Optical Pumping of Potassium and Rubidium. *47th Ann. Meet. APS DAMOP.* **61**, 8 (2016).
21. Alcock, C. B., Itkin, V. P. & Horrigan, M. K. Vapour Pressure Equations for the Metallic Elements: 298–2500 K. *Can. Metall. Quart.* **23**, 309–313 (1984).
22. Ito, Y., Sato, D., Kamada, K. & Kobayashi, T. Optimal densities of alkali metal atoms in an optically pumped K-Rb hybrid atomic magnetometer considering the spatial distribution of spin polarization. *Opt. Express* **24**, 015391 (2016).
23. Jau, Y. Y., Miron, E., Post, A. B., Kuzma, N. N. & Happer, W. Push-pull optical pumping of pure superposition states. *Phys. Rev. Lett.* **93**, 160802 (2004).
24. Shang, H. N., Quan, W., Chen, Y., Li, Y. & Li, H. The Measuring Method of Atomic Polarization of Alkali Metal Vapor Based on Optical Rotation and the Analysis of the Influence Factors. *Spectrosc. Spect. Anal.* **36**, 305–309 (2016).
25. Babcock, E. *et al.* Hybrid Spin-Exchange Optical Pumping of ^{3}He. *Phys. Rev. Lett.* **91**, 123003 (2003).
26. Gibbs, H. M. & Hull, R. J. Spin-Exchange Cross Sections for Rb^{87}-Rb^{87} and Rb^{87}-Cs^{133} Collisions. *Phys. Rev.* **153**, 132–151 (1967).
27. Ressler, N. W., Sands, R. H. & Stark, T. E. Measurement of Spin-Exchange Cross Sections for Cs^{133}, Rb^{87}, Rb^{85}, K^{39}, and Na^{23}. *Phys. Rev.* **184**, 102–118 (1969).
28. Shao, W. J., Wang, G. D. & Hughes, E. W. Measurement of spin-exchange rate constants between ^{129}Xe and alkali metals. *Phys. Rev. A* **72**, 022713 (2005).
29. Ghosh, R. K. & Romalis, M. V. Measurement of spin-exchange and relaxation parameters for polarizing ^{21}Ne with K and Rb. *Phys. Rev. A* **81**, 043415 (2010).
30. Quan, W., Li, Y. & Liu, B. Simultaneous measurement of magnetic field and inertia based on hybrid optical pumping. *Europhys. Lett.* **110**, 60002 (2015).
31. Aleksandrov, E. B., Balabas, M. V., Vershovskii, A. K., Okunevich, A. I. & Yakobson, N. N. Spin-exchange broadening of magnetic-resonance line of potassium atoms. *Opt. Spectrosc.* **87**, 329–334 (1999).
32. Vliegen, E. *et al.* Faraday rotation density measurements of optically thick alkali metal vapors. *Nucl. Instrum. Methods Phys. Res. A* **460**, 444–450 (2001).
33. Walker, T. G. & Happer, W. Spin-exchange optical pumping of noble-gas nuclei. *Rev. Mod. Phys.* **69**, 629–642 (1997).
34. Bhaskar, N. D., Pietras, J., Camparo, J., Happer, W. & Liran, J. Spin Destruction in Collisions between Cesium Atoms. *Phys. Rev. Lett.* **44**, 930–933 (1980).
35. Kadlecek, S., Anderson, L. W. & Walker, T. Measurement of potassium-potassium spin relaxation cross sections. *Nucl. Instr. Meth. Phys. Res.* **402**, 208–211 (1998).
36. Chen, Y. *et al.* Spin-exchange collision mixing of the K and Rb ac Stark shifts. *Phys. Rev. A* **94**, 052705 (2016).
37. Budker, D. *et al.* Resonant nonlinear magneto-optical effects in atoms. *Rev. Mod. Phys.* **74**, 1153–1201 (2002).
38. Fang, J. C. & Qin, J. Advances in Atomic Gyroscopes: A View from Inertial Navigation Applications. *Sensors* **12**, 6331–6346 (2012).
39. Fang, J. C., Li, R. J., Duan, L. H., Chen, Y. & Quan, W. Study of the operation temperature in the spin-exchange relaxation free magnetometer. *Rev. Sci. Instrum.* **86**, 073116 (2015).
40. Appelt, A. *et al.* Theory of spin-exchange optical pumping of ^{3}He and ^{129}Xe. *Phys. Rev. A* **58**, 1412–1439 (1998).
41. Franz, F. A. & Volk, C. Electronic spin relaxation of the $4^2S_{1/2}$ state of K induced by K-He and K-Ne collisions. *Phys. Rev. A* **26**, 85–92 (1982).
42. Franz, F. A. & Volk, C. Spin relaxation of rubidium atoms in sudden and quasimolecular collisions with light-noble-gas atoms. *Phys. Rev. A* **14**, 1711–1728 (1976).
43. Franz, F. A. & Sooriamoorthi, C. E. Spin relaxation within the $6^2P_{1/2}$ and $6^2S_{1/2}$ states of cesium measured by white-light optical pumping. *Phys. Rev. A* **10**, 126–140 (1974).
44. Silver, J. A. Measurement of atomic sodium and potassium diffusion coefficients. *J. Chem. Phys.* **81**, 5125–5130 (1984).
45. Savukov, I. M. & Romalis, M. V. Effects of spin-exchange collisions in a high-density alkali-metal vapor in low magnetic fields. *Phys. Rev. A* **71**, 023405 (2005).
46. Kornack, T. W., Smullin, S. J., Lee, S. K. & Romalis, M. V. A low-noise ferrite magnetic shield. *Appl. Phys. Lett.* **90**, 223501 (2007).
47. Kubo, R. The fluctuation-dissipation theorem. *Rep. Prog. Phys.* **29**, 255–284 (1966).
48. Quan, W., Lv, L. & Liu, B. Q. Modeling and Optimizing of the Random ASG Drift Based on the Atomic Spin Gyroscope. *Rev. Sci. Instrum.* **85**, 113104 (2014).
49. Quan, W., Liu, Y. & Chen, Y. Coating Qualities Evaluation for Alkali-Metal Atomic Vapor Cells Based on Frustrated Total Internal Reflection. *Chin. Phys. Lett.* **31**, 030701 (2014).
50. Quan, W. *et al.* Far off-resonance laser frequency stabilization using multipass cells in Faraday rotation spectroscopy. *Appl. Optics* **55**, 2503–2507 (2016).
51. Quan, W. *et al.* Locking distributed feedback laser diode frequency to gas absorption lines based on genetic programming. *Opt. Eng.* **56**, 016106 (2017).

52. Quan, W., Wei, K. & Li, H. R. Precision measurement of magnetic field based on the transient process in a K-Rb-^{21}Ne co-magnetometer. *Opt. Express* **25**, 8470–8483 (2017).
53. Qi, R., Yu, X. L., Li, Z. B. & Liu, W. M. Non-Abelian Josephson effect between two F = 2 spinor Bose-Einstein condensates in double optical traps. *Phys. Rev. Lett.* **102**, 185301 (2009).
54. Ji, A. C., Sun, Q., Xie, X. C. & Liu, W. M. Josephson effect for photons in two weakly linked microcavities. *Phys. Rev. Lett.* **102**, 023602 (2009).
55. Ji, A. C., Xie, X. C. & Liu, W. M. Quantum magnetic dynamics of polarized light in arrays of microcavities. *Phys. Rev. Lett.* **99**, 183602 (2007).
56. Chen, Y. *et al.* Spin exchange broadening of magnetic resonance lines in a high-sensitivity rotating K-Rb-^{21}Ne co-magnetometer. *Sci. Rep.* **6**, 36547 (2016).
57. Griffith, W. C., Jimenez-Martinez, R., Shah, V., Knappe, S. & Kitching, J. Miniature atomic magnetometer integrated with flux concentrators. *Appl. Phys. Lett.* **94**, 023502 (2009).
58. Wildermuth, S. *et al.* Sensing electric and magnetic fields with Bose-Einstein condensates. *Appl. Phys. Lett.* **88**, 264103 (2006).

Acknowledgements

Author Contributions

J.H.L. and W.M.L. proposed the ideas. J.H.L. interpreted physics, performed the theoretical as well as the numerical calculations and wrote the main manuscript. D.Y.J., L.L.W., Y.L., W.Q., J.C.F. and W.M.L. checked the calculations and the results. All of the authors reviewed the manuscript.

Additional Information

Competing Interests: The authors declare that they have no competing financial interests.

Publisher's note: Springer Nature remains neutral with regard to jurisdictional claims in published maps and institutional affiliations.